JAAS

PAPER

View Article Online
View Journal | View Issue

Cite this: *J. Anal. At. Spectrom.*, 2018, **33**, 1057

Simultaneous measurement of Re–Os and S isotopic compositions of sulfur-bearing minerals using a Carius tube digestion-based N-TIMS and MC-ICP-MS approach

Shengling Sun, [a] Jie Li,*[a] Le Zhang, [a] Lu Yin [ab] and Jing Zhang[ab]

Received 16th January 2018
Accepted 26th April 2018

DOI: 10.1039/c8ja00014j

rsc.li/jaas

This study reports an improved procedure for the simultaneous determination of Re–Os and S isotopic compositions of sulfur-bearing minerals using negative thermal ionization mass spectrometry (N-TIMS) and multicollector-inductively coupled plasma-mass spectrometry (MC-ICP-MS), respectively. This approach uses a Carius tube digestion technique during inverse aqua regia digestion to avoid the incomplete decomposition of sulfide minerals and the partial loss of S and Os during acid digestion. The sequential separation and purification of S and Re from sample matrix elements is undertaken after Os separation by CCl_4 solvent extraction and utilizes a two-stage tandem column setup using cation and anion exchange resins. Sulfur is not adsorbed onto either of the cation or anion exchange resin columns and can be directly eluted using 0.1 mol L^{-1} HNO_3, whereas Re is adsorbed onto the anion exchange resin column. This approach allowed the quantitative recovery of S (99.8%) and Re (99.7%), and the efficient removal of matrix elements from the final purified sample. The $\delta^{34}S$ values of IAEA S-2, S-3, and IAPSO seawater standards determined during this study (calibrated using the IAEA S-1 standard) are consistent with the certified values and are of higher precision than the values obtained using conventional analytical techniques. Our approach can also be used with different kinds of sulfide minerals. This combined Re–Os–S isotopic analysis provides useful information on the timing of ore deposit formation and constrains the source of the ore-forming fluid material. This approach also allows the determination of Re–Os and S isotopic compositions of single sample digestion, thereby avoiding problems with sample heterogeneity that can arise when comparing S and Re–Os isotopic data generated by conventional approaches.

1. Introduction

The radioactive decay of rhenium-187 to osmium-187 ($t_{1/2}$ = 41.6 Ga) is a unique geochronometer in which both parent and daughter elements have siderophile and chalcophile affinities. This means that the Re–Os isotope system is a powerful tool for the dating of sulfide minerals.[1–7] In addition to geochronology, the Re–Os isotopic compositions of sulfide minerals may provide insights into the sources of metals in ore deposits, as different types of sources may have different Re–Os isotopic compositions.[4] Sulfur isotopes are also an important tracer for sulfide minerals as a result of the chalcophile, siderophile, and volatile behavior of this element. Consequently, the sulfur isotopic compositions of sulfide ores can provide information on the sources of sulfur and metals within ore deposits, helping to constrain the sulfide precipitation mechanisms that generate economic mineralization.[8–11] In addition, sampling at a sufficient spatial resolution can lead to the identification of sulfur isotopic gradients that in turn may provide vectors toward thermal centers of fluid upwelling or provide information on the oxidation state and activity of sulfur within ore-forming fluids. All this means that a combined Re–Os and S isotope analytical approach can provide valuable insights into the timing of formation, sourcing, and precipitation of sulfide minerals.

The increased use of the Re–Os system over the past two decades has been assisted by advances in measurement sensitivity and analytical accuracy. High-precision Re–Os analysis is invariably undertaken using negative thermal isotope dilution mass spectrometry (N-TIMS).[12] However, accurate Re–Os isochrons require the full equilibration of Re and Os within both the spikes used and during sample digestion.[13] Carius tube digestion methods cause the oxidation of Re and Os to their highest valence states by the use of inverse aqua regia, allowing the complete chemical equilibration of the sample with the Re and Os spikes for isotope dilution analysis. In addition, this method can prevent the loss of volatile Os oxides (OsO_4).[14]

[a]*State Key Laboratory of Isotope Geochemistry, Guangzhou Institute of Geochemistry, Chinese Academy of Sciences, Guangzhou, 510640, China. E-mail: jieli@gig.ac.cn; Tel: +86 2085290119*

[b]*University of Chinese Academy of Sciences, Beijing 100049, China*

Sulfur isotope ratio measurements are undertaken on SO_2 or SF_6 and are conventionally performed by either gas source-isotope ratio mass spectrometry (GS-IRMS) or by online elemental analysis-isotope ratio mass spectrometry (EA-IRMS).[15–17] The complex and multistep sample preparation methods used to convert various S-containing species from geological, biological, and environmental matrices into SO_2 or SF_6 can cause additional S isotopic fractionation or contamination by the reagents employed.[18] These difficulties have limited the use of $\delta^{34}S$ values, but continuous flow methods are now changing this situation.[19–22] The introduction of multi collector-inductively coupled plasma-mass spectrometry (MC-ICP-MS) technology over the past decade has led to this approach being used for sulfur isotopic analysis.[23–29] The high ion yields (combining ionization efficiency and sample usage) and the low detection limits of this approach mean that the sample sizes used for MC-ICP-MS analysis are at least an order of magnitude smaller than those required for the SO_2 and SF_6 methods.[25] In addition, MC-ICP-MS analysis yields much more accurate $^{33}S/^{32}S$ and $^{34}S/^{32}S$ ratios than the measurements undertaken on SO_2.[25] Nevertheless, the use of MC-ICP-MS is still very rare for S isotopes,[24] with gaseous sources dominating the community.[18–22,30–40]

Although various analytical methods for Re–Os and S isotope measurements have been developed, few studies have considered simultaneous Re–Os and S isotopic determination approaches that use single sulfide sample aliquots. Here, we present a new analytical procedure that allows the simultaneous measurement of Re–Os and S isotopic compositions of single sulfide mineral digestions. This approach uses a Carius tube digestion technique to avoid the loss of volatile SO_2 and OsO_4 during inverse aqua regia digestion and the associated oxidation of sulfide minerals. This digestion is followed by separation, purification, and measurement of Re–Os and S isotopic compositions by N-TIMS and MC-ICP-MS, respectively. This approach was verified using a wide variety of sulfide minerals, including pyrite, chalcopyrite, chalcocite, and molybdenite, reflecting the various possible uses of this methodology in ore deposit studies.

2. Experimental

2.1 Chemicals and reagents

All sample preparation was undertaken in an ultra-clean laboratory. Ultra-pure water (resistivity of 18.25 MΩ cm at 25 °C) was purified using a Millipore Milli-Q system and was used during all experimental procedures. In addition, the HCl, HBr, and HNO_3 reagents used during this study were purified using Savillex DST-1000 sub-boiling stills. The HNO_3 used for sample digestion was vigorously bubbled before being distilled to remove any volatile OsO_4. Ultrapure HPLC grade CCl_4 was used without further purification. Finally, prior to use, PFA vials and round-bottomed Carius tubes (25 mm interior diameter and 22 mm height) were immersed and soaked in aqua regia (50%, v/v) before being heated at 350 °C for 6 h, rinsed with Millipore water, and then dried.

Eichrom 100–200 mesh H^+ AG50W-X8 cation and 100–200 mesh AG1-X8 Cl^- anion exchange resins were pre-cleaned twice using HCl (50%, v/v) and Millipore water to reduce resin blanks before being stored in 6 mol L^{-1} HCl. The resins were subsequently loaded into 8 × 40 mm 10 mL Poly-Prep columns (Bio-Rad Laboratories) before being serially washed with 3 mL of 6 mol L^{-1} HCl and then with 10 mL of Millipore water until the pH of the effluent liquid was neutral, with final equilibration using 6 mL of 0.1 mol L^{-1} HNO_3.

2.2 Preparation of sulfur reference standards

The reliability of the isotopic measurement approach used during this study was verified and calibrated using three Ag_2S international reference materials from the International Atomic Energy Agency (IAEA; IAEA S-1, S-2, and S-3) and an IAPSO seawater standard from OSIL. These reference materials were used because they cover a wide range of sulfur isotopic compositions (−32‰ to +22‰) and are widely available. In addition, an artificially prepared Ag_2S standard (IAEA S-1) with a $\delta^{34}S_{VCDT}$ of −0.3‰ is now recommended for use as an international standard reference material. Solutions of these IAEA standards were made using the protocol outlined by Craddock *et al.*[23] This approach used 50 mg of each sulfur reference material (IAEA S-1, S-2, and S-3), which was accurately weighed into 15 mL Savillex PFA beakers cleaned with concentrated HCl and then with Milli-Q water. These reference materials were then dissolved in 5 mL of 50% HNO_3 (v/v) before being slowly dried on a hot plate at 70 °C. The dried $AgNO_3$ and S were then dissolved in 3 mL of concentrated HNO_3 and 2 mL of 50% HCl (v/v) before being dried again at 70 °C to yield H_2SO_4 and AgCl. The resulting white crystalline solids were mixed with 4 mL of 2% HNO_3 before being transferred to a centrifuge tube. The insoluble material (*i.e.*, AgCl) was separated from the solution by centrifugation before the standard solutions obtained from the liquid supernatant were diluted with the required amount of 2% HNO_3 to yield a final stock solution containing 20 μg mL^{-1} S that was ready for isotopic analysis. The reactions mentioned above and used during this preparation are as follows:

$$3Ag_2S + 8HNO_3\ (\text{dilute}) = 6AgNO_3 + 3S\downarrow + 2NO\uparrow + 4H_2O$$

$$S + 6HNO_3\ (\text{concentrated}) = H_2SO_4 + 6NO_2\uparrow + 2H_2O$$

$$AgNO_3 + HCl = AgCl\downarrow + HNO_3$$

2.3 Preparation and chemical purification of sulfide minerals

Prior to analysis, 20–500 mg of sulfide mineral sample powder and appropriate amounts of ^{185}Re and ^{190}Os spikes were digested in Carius tubes using inverse aqua regia (2 mL of concentrated HCl and 6 mL of concentrated HNO_3) for 24 h at 220 °C. Osmium was subsequently separated by solvent extraction using CCl_4 with subsequent HBr back-extraction and purification by microdistillation. The remaining S- and Re-bearing solution was evaporated to incipient dryness at 100 °C

before 0.5 mL of 6 mol L^{-1} HNO_3 was added and the mixture was heated to dryness, with this step being repeated to ensure the conversion of hydrochlorides to nitrates. The resulting residue was dissolved by the addition of 1 mL of 0.1 mol L^{-1} HNO_3. This solution was then ready for ion exchange chromatography to separate S and Re from the remaining matrix.

Ion exchange chromatography used 1 mL of the dissolved sample solution that was loaded onto the prepared cation column, with the effluent liquid from the anion column being collected after ion exchange. Passing the S- and Re-bearing elution solution through the prepared anion column caused ReO_4^- to be adsorbed onto the anion resin whereas SO_4^{2-} passed through the anion exchange column without adsorption. A further 10 mL of 0.1 mol L^{-1} HNO_3 was added to the cation column to ensure the total elution of Re and S, and to ensure the complete recovery of S from the anion column. The eluent was simultaneously collected and combined with the effluent liquid before a small aliquot of the S eluted solution was diluted with 2% HNO_3 to give a stock containing 20 μg mL^{-1} of S that could be directly analyzed by MC-ICP-MS.

The cation column was removed after this ion exchange and the anion column was eluted with 7 mL of 2 mol L^{-1} HNO_3 to remove the remaining matrix from the resin (especially Mo). The anion column was then eluted with 10 mL of 3 mol L^{-1} HNO_3 for the collection of Re. The Re eluted solution was then evaporated before being diluted with 2 mL of 2% HNO_3, with the resulting dilute solution used for the analysis of Re by ICP-MS. The resulting fractions of Os, S and Re were measured by N-TIMS, MC-ICP-MS, and ICP-MS, respectively. The separation and purification approaches are summarized in Scheme 1.

2.4 Instrumentation

Osmium isotope ratios were measured as OsO_3^- ions using the electron multiplier mode of a Thermo-Finnegan Triton N-TIMS

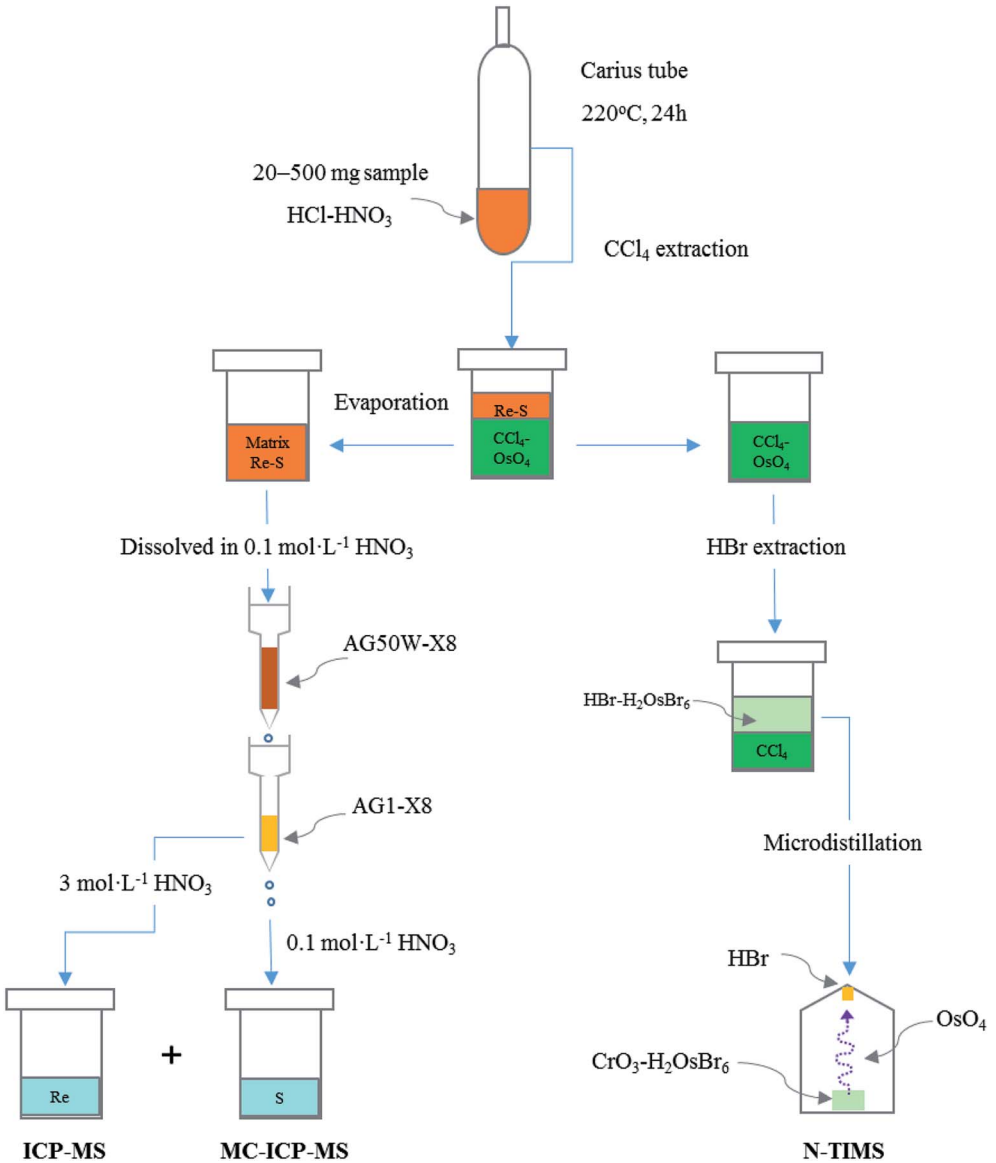

Scheme 1 Process used to separate and purify Re–Os–S from sulfide samples an d standards during this study.

instrument[41,42] at the State Key Laboratory of Isotope Geochemistry, Guangzhou Institute of Geochemistry, Chinese Academy of Sciences (GIGCAS), Guangzhou, China. Prior to analysis, the samples were loaded at *ca.* 0.6 A onto high-purity Pt filaments (99.999%, 1 × 0.025 mm) that had previously been outgassed in air for 30 minutes at *ca.* 4 A. Complete evaporation was followed by covering of the sample with 10 μg of Ba from a 10 000 ppm $Ba(OH)_2$ solution. High-purity O_2 gas was introduced into the ion source *via* a leak valve to maintain a pressure of *ca.* 3×10^{-7} mbar. Osmium isotope ratios were determined by peak jumping on masses 235, 236, 237, 238, and 240 of the molecular ion OsO_3^-. Mass 233 (corresponding to $^{185}Re^{16}O_3^-$) was measured throughout each run to monitor and correct for potential $^{187}Re^{16}O_3^-$ interference on $^{187}Os^{16}O_3^-$ (mass 235). The resulting data were corrected offline to remove oxygen and spike contributions.

Rhenium concentrations were determined using ICP-MS (Thermo Scientific X Series 2) with a conventional low-volume quartz impact bead spray chamber housing a Peltier cooled (3 °C) 0.4 mL min^{-1} borosilicate nebulizer (Micromist GE). Ion lens settings, nebulizer gas flow rates, and torch positions were all optimized daily using a 10 ng mL^{-1} tuning In–Ce standard solution to obtain high instrumental sensitivities and low oxide production levels. This approach did not use a peristaltic pump, as the free aspiration of the nebulizer yielded better signal stability. Additional details of the ICP-MS analysis method are given by Li *et al.*[43]

All S isotopic compositions were determined using MC-ICP-MS (Thermo Fischer Neptune Plus) at the State Key Laboratory of Isotope Geochemistry, GIGCAS, Guangzhou, China. Typical instrument setting, measurement, and data acquisition parameters are given in Table 1. Some other tuning parameters were adjusted on a day-to-day basis to optimize the sensitivity and stability of the signals.

Isotope ratio measurements were undertaken in high-resolution mode to remove molecular interferences resulting from the presence of oxygen species. A standard-sample bracketing (SSB) approach was used for mass bias correction, where the measurement of a sample is bracketed by measurements of a standard immediately before and after the sample. The fractionation factor derived from instrumental mass bias can be determined for the standards using linear interpolation between the measurements of two neighboring standard analyses, with this bias then being used to correct the composition of the unknown sample. As such, the average of the standard isotopic ratio values determined using this SSB method is used to calculate the delta notation-based composition of the sample. Sulfur isotopic measurements were undertaken at masses ^{32}S, ^{33}S, and ^{34}S (monitored at the L_3, C, and H_3 Faraday cups, respectively) and were determined to be free of O_2 interference on the low mass side of the plateau of the interfering species. All measurements were undertaken using an integration time of 4.2 seconds with data acquisition undertaken for 40 individual measurements. Mean isotopic ratios of the IAEA S-1 bracketing standard and samples evaluated using Neptune software were used for calculating $\delta^{34}S$ values as follows:

$$\delta^{34}S = \delta\left(\frac{^{34}S}{^{32}S}\right) = \left[\frac{\left(^{34}S/^{32}S\right)_{sample}}{\left(^{34}S/^{32}S\right)_{standard}} - 1\right] \times 1000 \quad (1)$$

The intensities of these sulfide samples closely match the signal intensity of the IAEA S-1 bracketing standard (within ~10%). Washing during analytical sessions was carried out using 2% ultra-pure HNO_3 solutions with rinse times of 2–3 min between samples. This yielded a background ^{32}S signal intensity of ≤0.5 mV, meaning that no background correction was necessary because of the generally small background contributions (≤0.04‰) relative to the signal intensities of the sample analyte on ^{32}S.

3. Results and discussion

3.1 Two-stage tandem column for the separation and purification of Re and S

The measurement of S isotopic ratios by MC-ICP-MS relies on the SSB method outlined above, and this approach assumes that instrumental mass bias is identical during the analysis of both standards and samples. However, instrumental mass bias can be affected by matrix impurities (typically referred to as the "matrix effect"), meaning that samples must be treated to remove matrix elements prior to analysis. Two types of resins can be used to separate S from matrix elements: an AG50-X8 cation exchange resin or an AG1-X8 anion exchange resin.[23–25,44] After inverse aqua regia digestion, S and Re are generally present in anionic forms as SO_4^{2-} and ReO_4^-, respectively, neither of which are adsorbed by cation resins, whereas major matrix elements such as Zn, Fe, and Cu are quantitatively adsorbed by these resins. Although this technique is simple, some matrix elements (*e.g.*, Zr, Hf, Mo, and W) are generally still present after cation exchange separation. The anionic forms of

Table 1 Typical parameters and the setup used during Neptune Plus MC-ICP-MS analysis

Neptune instrument parameter	Value	Measurement parameter	Value
RF power [W]	1263.0	Cup configuration	^{32}S(L3), ^{33}S(C), ^{34}S(H3)
Cool gas [L min^{-1}]	16.7 (Ar)	Resolution mode	High (entrance slit)
Aux gas [L min^{-1}]	1.0 (Ar)	Sample uptake rate [μL min^{-1}]	50
Sample gas [L min^{-1}]	1.0 (Ar)	Integration time	4.2 s integration time per cycle, 40 cycles per analysis
Ion getter press [mbar]	2.77×10^{-8}	Wash time	Approximately 2–3 min with 2% HNO_3 solutions before every standard and sample

SO_4^{2-} and ReO_4^- could also adsorb onto anion exchange resins, but SO_4^{2-} has only a weak affinity for anion exchange resins, meaning that quantitative adsorption is difficult.[25] The separation of S and Re from matrix elements was undertaken using a tandem column setup in this study, where the eluent from the cation exchange column was allowed to directly pass through the anion exchange column. This approach does not extract S into either cation or anion exchange resins, whereas Re is retained within the anion exchange resin column, allowing matrix and interfering elements to be removed from the eluted solutions.

Each stage of column purification was optimized using a synthetic standard solution of Re, S, and matrix elements (1000 μg mL^{-1} of Mo–Fe–Cu–Ni–Mn–Zn, 320 μg mL^{-1} of S, and 200 ng mL^{-1} of Re). The chromatographic procedure used columns containing 2 mL of the AG 50W-X8 cation exchange resin and 1 mL of the AG1-X8 anion exchange resin. The ReO_4^- in the solution was retained within the anion exchange resin column whereas SO_4^{2-} was not, meaning that SO_4^{2-} could be eluted from the two-stage tandem column using 10 mL of 0.1 mol L^{-1} HNO_3. The continued elution of the anion resin column used 7 mL of 2 mol L^{-1} HNO_3 and 12 mL of 3 mol L^{-1} HNO_3 to remove Mo and collect Re, respectively. The elution profiles and chemical yields for our tandem column separation procedure, using 0.1 mol L^{-1} HNO_3 as the eluent, are shown in Fig. 1. As expected, the majority of the major elements (*e.g.*, Fe, Cu, Ni, Mn, and Zn) were generally retained within the cation column, yielding very low residual concentrations within the analyte solution; consequently, the recoveries of Fe, Cu, Ni, Mn, and Zn are not shown in Fig. 1. The S recovery rate was >99.8% when eluted with 10 mL of 0.1 mol L^{-1} HNO_3 solution. The interference of Mo on Re, an essential consideration when analyzing molybdenite samples containing high concentrations of Mo, was removed by washing the anion resin column with 7 mL of 2 mol L^{-1} HNO_3 to remove Mo. The column was then eluted using 3 mol L^{-1} HNO_3 to collect a pure Re fraction. Using 10 mL of 3 mol L^{-1} HNO_3 eluent assured the complete release of Re from the anion resin, yielding a Re recovery rate as high as 99.7%; consequently, the later analysis of sulfide samples used this approach with 10 mL of 0.1 mol L^{-1} HNO_3 for loading and eluting S, 7 mL of 2 mol L^{-1} HNO_3 for the removal of Mo, and 10 mL of 3 mol L^{-1} HNO_3 for the collection of Re.

3.2 Precision and accuracy of S isotope ratio measurements by MC-ICP-MS

The use of MC-ICP-MS to determine the $\delta^{34}S$ values of sulfur-containing solutions is hindered by the fact that isobaric interferences and matrix effects can strongly influence the accuracy and precision of $\delta^{34}S$ values. Polyatomic ions, specifically the hydroperoxide group ($^{16}O^{16}O^+$, $^{16}O^{16}O^1H^+$, and $^{16}O^{17}O^1H^+$), are produced by molecular species generated within the argon plasma and at the interface between the ion source and the mass spectrometer.[23,45,46] These polyatomic ions cannot be resolved at low mass resolutions; *e.g.*, the analysis of $^{34}S^+$ in an H_2O matrix has an interference associated with $^{16}O^{18}O^+$ where a mass resolution of ~1300 is required to resolve this polyatomic interference. Mass resolutions between 2000 and 5000 are required for the majority of polyatomic

Table 2 Isobaric interferences on sulfur isotope masses

Isotope	Amu.	Abundance (%)	Interference	$m/\Delta m$
^{32}S	31.9721	94.93	$^{16}O^{16}O$	1801
			$^{16}O^{17}O$	1461
^{33}S	32.9715	0.76	$^{16}O^{16}O^1H$	1260
			$^{32}S^1H$	3907
			$^{16}O^{18}O$	1297
^{34}S	33.9679	4.29	$^{16}O^{17}O^1H$	1000
			$^{33}S^1H$	2977

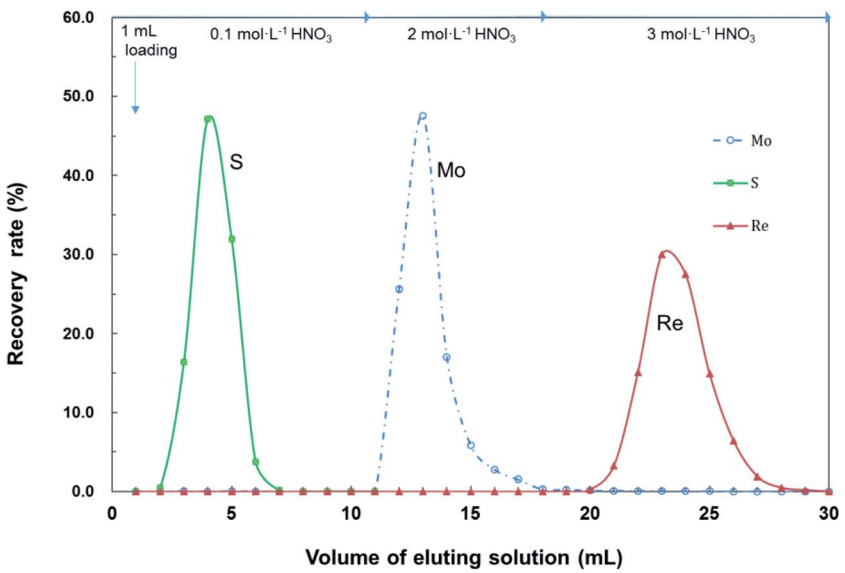

Fig. 1 Elution curves for Re, Mo, and S obtained for multi-element solutions.

interferences (Table 2), with isobaric interferences from oxygen species removed by the use of medium-to-high mass resolutions and interference-free plateaus to detect sulfur isotopes.

The high resolution peak shapes for 2 μg mL^{-1} of the IAEA S-1 sulfur standard in 2% HNO_3 (Fig. 2a) and the 2% HNO_3 blank (Fig. 2b) obtained during MC-ICP-MS analysis are shown in Fig. 2. The three sulfur isotopes were simultaneously detected by MC-ICP-MS in three Faraday collectors, namely L_3 (^{32}S), C (^{33}S), and H_3 (^{34}S). The resulting signal intensities of ^{33}S and ^{34}S were multiplied by 56.90 and 130.05, respectively, to match the signal intensity of ^{32}S (Fig. 2). Clear interference peaks were observed on the high mass side (>32.96 u) by comparing Fig. 2a and b, with these interferences identified as $^{16}O_2^+$ on $^{32}S^+$, $^{32}S^1H^+$ and $^{16}O^{17}O^+$ on $^{33}S^+$, and $^{16}O^{18}O^+$ on $^{34}S^+$. The lower mass shoulder of the peak is free of interference and is the location of the measurement of the signal intensities of the sulfur isotopes ^{32}S, ^{33}S, and ^{34}S. An interference-free plateau with a width less than 0.005 u is present between masses 32.946 and 32.950 (Fig. 2c), with the exact position of the center cup set at 32.948 u for the following S isotopic analyses.

The long-term reproducibility of the isotopic measurements of the IAEA S-1 standard integrated over three independent analytical stages is shown in Fig. 3. The external reproducibility of the $\delta^{34}S$ values of this standard during the measurement period was within $\pm 0.06‰$ (2σ, $n = 65$). This is the same as the typical reproducibility of 0.08–0.15‰ (2σ) on $\delta^{34}S$ reported by

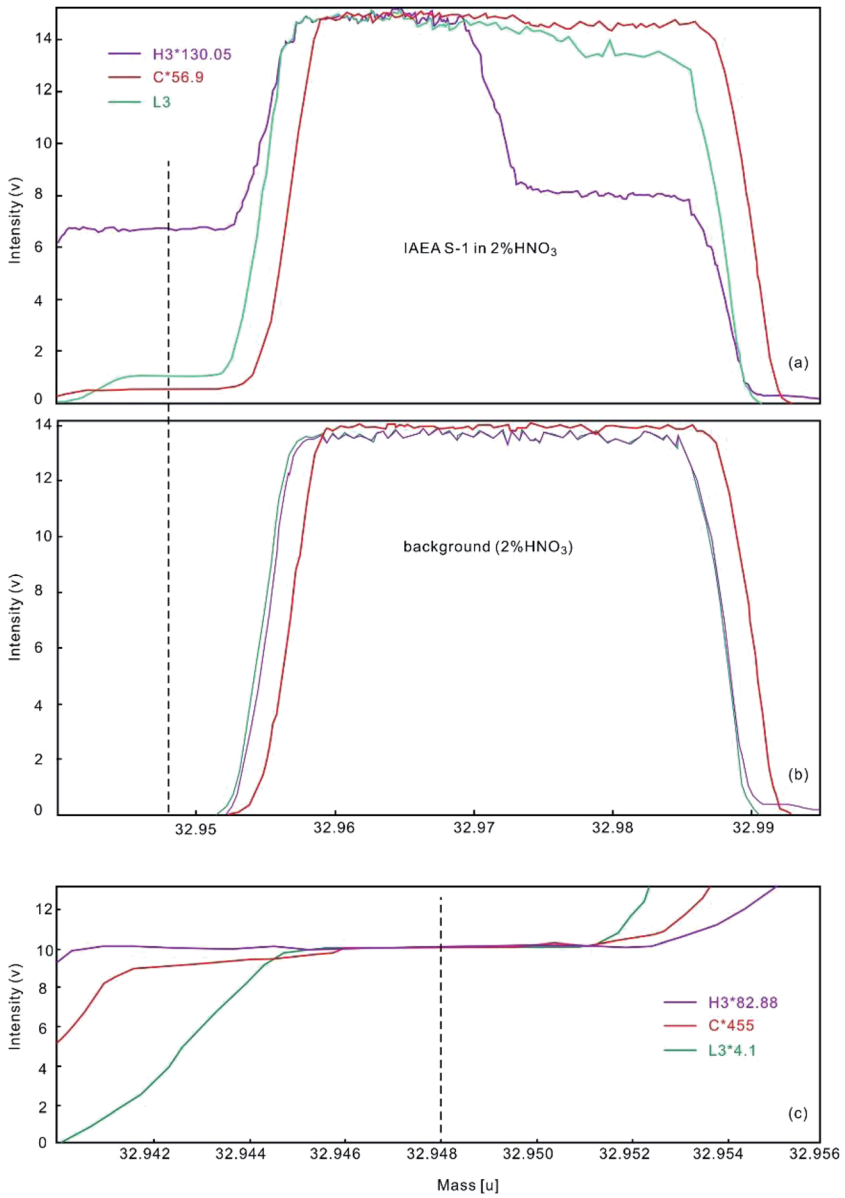

Fig. 2 Peak shapes for sulfur isotope species from IAEA S-1 (2 μg mL^{-1} of S) in 2% HNO_3 solution (a) and a sulfur-free 2% HNO3 blank (b). Beams were collected simultaneously using three Faraday cups, namely L3 (^{32}S), C (^{33}S), and H3 (^{34}S). The green line represents ^{32}S, the red line represents ^{33}S, and the purple line represents ^{34}S. Significant interference occurs on all sulfur masses, but the plateau on the lower mass indicates resolved interferences where sulfur isotopes could be detected (shown in (c)). The black vertical dashed lines mark the positions used for selected masses employing the C Faraday collector, as determined by the presence of an interference-free plateau.

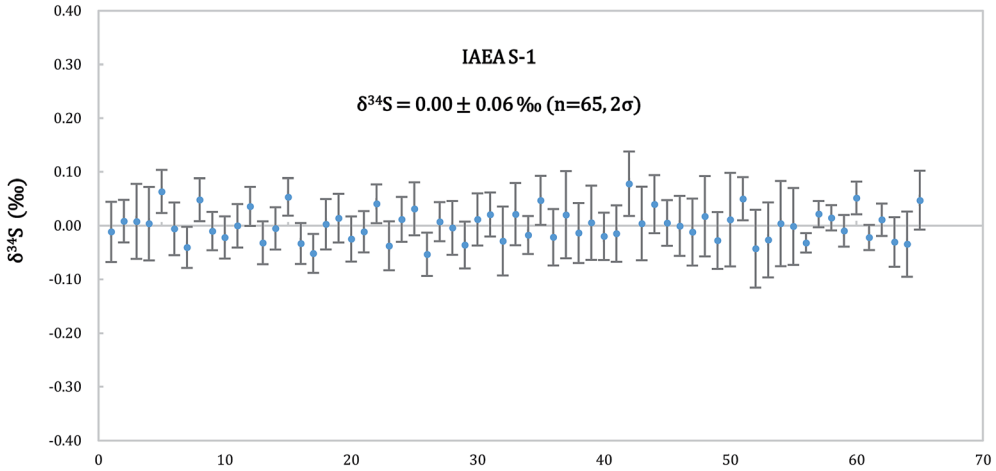

Fig. 3 Variability in $\delta^{34}S$ values obtained during replicate MC-ICP-MS measurement monitoring.

Paris *et al.* (2013 and 2014) using MC-ICP-MS measurements,[25,26] and is comparable to the uncertainty of 0.01–0.15‰ (1σ) reported by Labidi *et al.* (2014) for both IAEA and basalt standards, using a widely different chemistry and the SF_6 method.[31] These results indicate that the resulting $\delta^{34}S$ is of high precision, thereby validating this approach to determining solution S isotopic compositions using MC-ICP-MS in high-resolution mode.

The precision of the SBB sulfur isotope analysis was evaluated using IAEA S-2 and S-3 standard solutions, with IAEA S-1 being used without further purification as a reference standard to bracket the IAEA S-2 and IAEA S-3 standards. The mean $\delta^{34}S$ values and standard deviations (2σ) are shown in Fig. 4, where these values are compared with the previously reported values summarized in Table 3. The $\delta^{34}S$ values of +22.64‰ ± 0.11‰ (2σ, $n = 18$) and −32.16‰ ± 0.21‰ (2σ, $n = 9$) for the IAEA S-2 and IAEA S-3 standards analyzed during this study are in good agreement with the values reported in the references,[23,24,29,50,51] such as 22.26‰ ± 0.42‰ (2σ) and −32.29‰ ± 0.45‰ (2σ) provided by Das *et al.*,[24] respectively. As shown in Table 3, the results of IAEA S-2 and IAEA S-3 in our study are consistent with the values reported by Labidi *et al.* (2014)[31] and Ono *et al.* (2012),[22] using the SF_6 method. The approach used during this study, based on chemical separation and mass spectrometry, was further validated by repeated determinations of the $\delta^{34}S$ composition of the IAPSO seawater standard after separation and purification using the two-stage tandem column method outlined above. The IAPSO seawater standard analyzed during this study yielded $\delta^{34}S$ values of +21.45‰ ± 0.32‰ (2σ, $n = 15$) that again are similar to previously reported values determined by MC-ICP-MS (+21.11 ± 0.40‰ (ref. 24) and +21.19 ± 0.27‰ (ref. 23)). In terms of accuracy and precision, the results are in good agreement with the value (+21.15 ± 0.30‰; 2σ, $n = 180$) of modern seawater determined by means of the SF_6 method by Johnston *et al.*[47] Evidently, the measured $\delta^{34}S$ values of the standards (*i.e.*, IAEA S-2, IAEA S-3 and IAPSO seawater) analyzed during this study are also externally precise, yielding values of ±0.11‰, ±0.21‰, and ±0.32‰, agreeing with the published uncertainties for these standards.

3.3 Re–Os–S isotopic analysis of sulfide minerals

The aqua regia and two-stage tandem column approach outlined above was verified by the analysis of 13 sulfide minerals, including chalcopyrite, chalcocite, and pyrite samples as well as pyrrhotite and molybdenite standards. The Re and Os contents, and S isotopic compositions of these samples are given in Table 4. As expected, our analytical approach yields satisfactory S isotope values for the pyrrhotite sample YD136-206 (1.97‰ ± 0.25‰; 2σ) that are within the uncertainty of the $\delta^{34}S$ value (1.92‰ ± 0.34‰; 2σ) obtained by traditional IRMS methods, indicating that our approach does not introduce any artificial isotope fractionation (as a result of the loss of S) during chemical purification. The analysis of the JDC Jinduicheng molybdenite sample, a Chinese molybdenite reference material, yielded Re and ^{187}Os contents of 17.03 ± 0.05 μg g^{-1} and 24.79 ± 0.02 ng g^{-1}, respectively, as well as a calculated model age (138.8 ± 0.4 Ma) that is well within the error of the certified value published by Stein *et al.*[48] In addition, the $\delta^{34}S$ value (+4.43‰ ± 0.05‰; 2σ) determined for the JDC standard is well within the range of compositions (+4.2‰ to +4.5‰) for the Jinduicheng molybdenite reported by Huang *et al.*[49] These results demonstrate the accuracy and precision of the analytical approach outlined in this study, as well as the validity and reliability of the chemical procedure utilized here.

The $\delta^{34}S$ values for the sulfides analyzed during this study are variable, with values from +0.91‰ to +2.34‰ for the chalcopyrite samples, from −5.46‰ to −1.39‰ for the pyrite samples, and −11.01‰ to −10.66‰ for the chalcocite samples. These data indicate that these various types of mineralization are formed from different types of ore-forming fluids. The negative $\delta^{34}S$ values for the pyrite and chalcocite are indicative of sulfides containing elevated amounts of light sulfur isotopes, whereas the positive $\delta^{34}S$ values of the chalcopyrite are indicative of slight enrichments in heavy sulfur isotope (^{34}S). In addition, the $\delta^{34}S$ values of −11.01‰, −10.94‰, and −10.66‰ for the chalcocite samples indicate that this region has relatively uniform S isotopic compositions. The variable characteristics of the sulfur isotopic compositions most likely

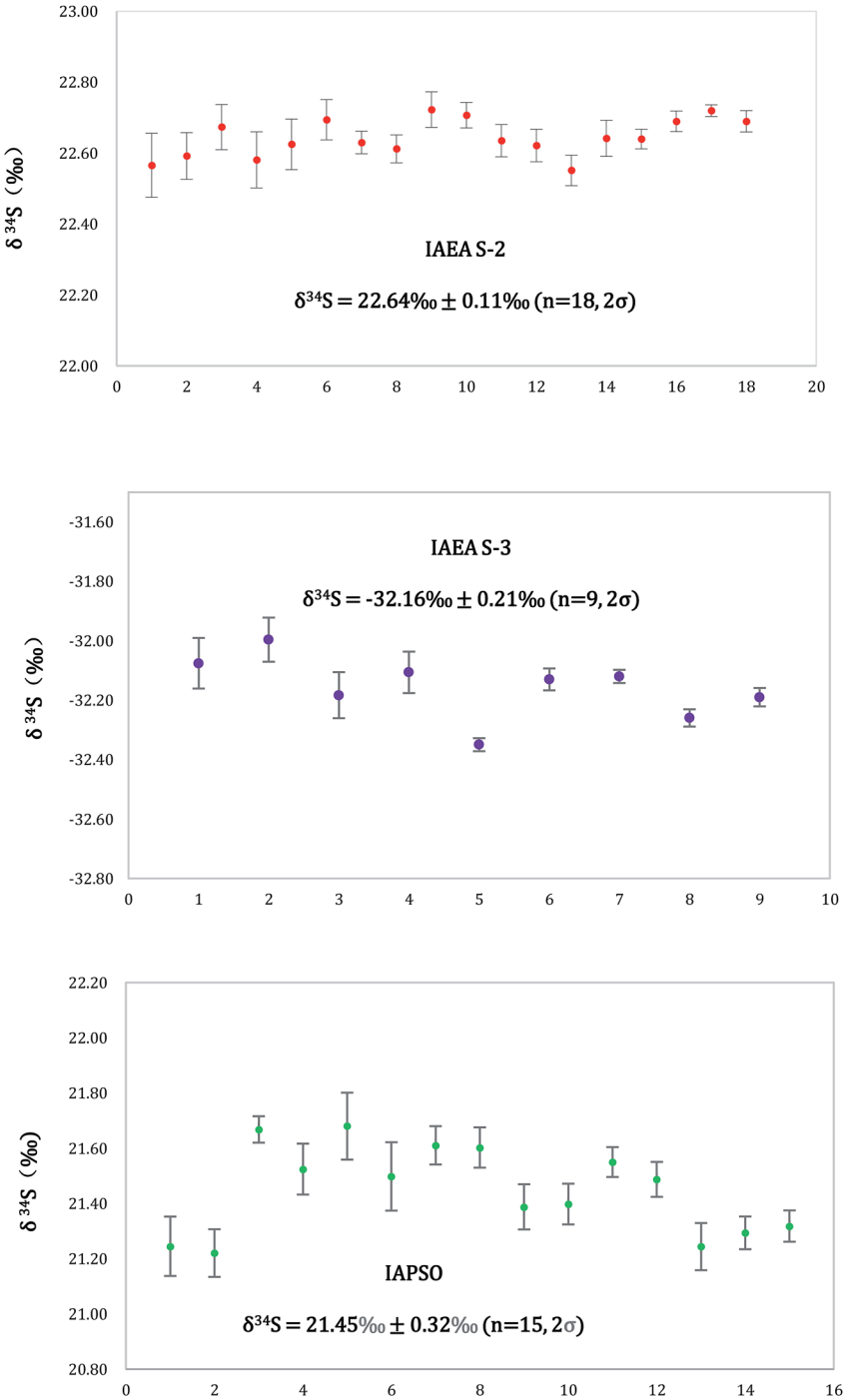

Fig. 4 $\delta^{34}S$ values for IAEA S-2, S-3, and IAPSO seawater standards analyzed during this study.

reflect changes under oxidizing and reducing conditions during ore formation.

The Re and Os concentrations of these sulfide minerals vary significantly from pg g^{-1} to ng g^{-1} levels, with the majority having low concentrations. Replicate analyses of the chalcopyrite, pyrite, and chalcocite samples yield highly variable Re, Os, and isotopic compositions (Table 4).

The four low-Os chalcopyrite samples (concentrations in pg g^{-1}) yield relatively radiogenic $^{187}Os/^{188}Os$ ratios of 32–278 and an isochron age of 208.6 ± 3.0 Ma. In comparison, the four pyrite samples have non-radiogenic $^{187}Os/^{188}Os$ ratio values (3–8) with high Os and low Re concentrations, whereas the three chalcocite samples have radiogenic $^{187}Os/^{188}Os$ ratios of 3–16 and contain higher concentrations of Re and lower concentrations of Os. The samples with high Os concentrations and radiogenic Os isotopic compositions reflect differences in Re contents or Re/Os ratios. The pyrite and chalcocite samples yield Re–Os isochron ages of 396.1 ± 6.2 Ma and 11.7 ± 2.3 Ma, respectively, as calculated using Isoplot (Fig. 5). These ages represent the timing of formation of these sulfides and most

Table 3 Comparison of $\delta^{34}S$ (in ‰) values for the IAEA S-2, IAEA S-3, and IAPSO seawater standards against the results of analysis of the IAEA S-1 standard[a]

Origin	S-2 (‰)	S-3 (‰)	Seawater (‰)
This study	+22.64 ± 0.11	−32.16 ± 0.21	+21.45 ± 0.32
Ding *et al.* (2001)[50]	+22.67 ± 0.15	−32.55 ± 0.12	n.a.
Craddock *et al.* (2008)[23]	+22.44 ± 0.43	n.a.	+21.19 ± 0.27
Das *et al.* (2012)[24]	+22.26 ± 0.42	−32.29 ± 0.45	+21.11 ± 0.40
Ono *et al.* (2012)[22]	+22.24 ± 0.27	−32.58 ± 0.20	+21.34 ± 0.13
Labidi *et al.* (2014)[31]	+22.33 ± 0.12	n.a.	n.a.
Johnston *et al.* (2014)[47]	n.a.	n.a.	+21.15 ± 0.30
Yu *et al.* (2017)[29]	+22.60 ± 0.19	−32.12 ± 0.18	n.a.

[a] n.a. = not analyzed.

likely the timing of formation of their associated ore deposits. Combining these age data with the geology of the sampling region interprets the S and Re–Os isotopic compositions of these sulfide minerals and provides more information and useful insights into metallogenesis. For example, a combination of S and Re–Os isotopic data can reveal the timing of metallogenesis and the source of ore-forming fluids, and provide insights into metal sources and the processes of ore formation.[52]

In summary, high-accuracy Re–Os concentrations and high-precision S isotopic data can be simultaneously obtained by the chemical and measurement approaches outlined above, indicating that these methods can be used for coupled S and Re–Os isotopic analysis of sulfides, which is particularly effective when applied to molybdenite.

3.4 Total procedural blanks

The sulfides analyzed during this study contain low concentrations of Re and Os, indicating that the analytical techniques and processes used to determine background concentrations need to be carefully considered to yield meaningful Re–Os isochron ages. The total procedural blanks resulting from digestion and purification are 2–5 pg for Re, 0.2–0.4 pg for Os, and 30–50 ng for S. The Re and Os total procedural blanks are at very low levels that are essentially the same as those obtained during previous research using standard techniques.[53] In addition, the sulfur total procedural blank is much lower than the value obtained using a cation exchange resin approach in a previous study (250 ng; Craddock *et al.*[23]). The lower total procedural blanks reported in this study represent the whole chemical procedure, including digestion and purification (Scheme 1), rather than representing single column chemistry blanks. Moreover, the S blank value for the two-stage tandem column used in this study is 17.25 ng S (*versus* 320 μg S used), which is close to that reported for an anion exchange resin (9–16 ng) by Das *et al.*[24] These low total procedural blanks indicate that the Re, Os, and S isotopic data obtained using this approach are reliable, thereby confirming the usability of the approaches outlined in this study.

Table 4 Re–Os–S compositions of the sulfide mineral samples analyzed during this study[a]

Sulfide mineral	Sample	Re (ng g^{-1})	2σ	Os (ng g^{-1})	2σ	$^{187}Os/^{188}Os$	2σ	$^{187}Re/^{188}Os$	2σ	$\delta^{34}S$ (‰)	2σ
Chalcopyrite	S-1	9.921	0.034	0.0236	0.0003	93.71	0.75	26 733	305	0.91	0.05
	S-2	25.82	0.69	0.0592	0.0003	192.8	1.0	54 921	1498	2.35	0.04
	S-3	4.242	0.036	0.0119	0.0001	32.82	0.22	9027	92	1.30	0.04
	S-4	33.67	0.67	0.0769	0.0004	278.9	1.5	78 781	1626	1.31	0.04
Pyrite	S-5	5.114	0.064	0.0531	0.0001	8.673	0.028	982	12	−5.46	0.05
	S-6	4.997	0.13	0.1026	0.0001	4.724	0.008	375	10	−4.06	0.05
	S-7	3.380	0.075	0.1221	0.0002	3.456	0.005	191	4	−3.58	0.04
	S-8	4.107	0.094	0.1545	0.0002	3.397	0.004	183	4	−1.39	0.08
Chalcocite	S-9	209.6	0.9	0.0610	0.0003	7.985	0.056	33 500	214	−10.94	0.04
	S-10	61.48	0.26	0.0411	0.0001	3.687	0.016	10 555	50	−10.66	0.05
	S-11	421.5	2.3	0.0833	0.0001	16.59	0.05	76 769	442	−11.01	0.04
Pyrrhotite	YD136-206	52.53	0.19	n.a.	n.a.	n.a.	n.a.	n.a.	n.a.	1.97	0.25
	Reference analysis by IRMS	n.a.	n.a.	n.a.	n.a.	n.a.	n.a.	n.a.	n.a.	1.92	0.34

Sulfide mineral	Sample	Re (μg g^{-1})	2σ	^{187}Re (μg g^{-1})	2σ	^{187}Os (ng g^{-1})	2σ	Model T (Ma)	2σ	$\delta^{34}S$ (‰)	2σ
Molybdenite	JDC	17.03	0.05	10.7	0.03	24.79	0.02	138.8	0.4	4.43	0.05
	Reference by Stein *et al.*[48]	17.33	0.05	10.89	0.03	25.13	0.09	138.3	0.6	n.a.	n.a.

[a] Decay constant of ^{187}Re (λ) = 1.666×10^{-11} per annum, n.a. = not analyzed.

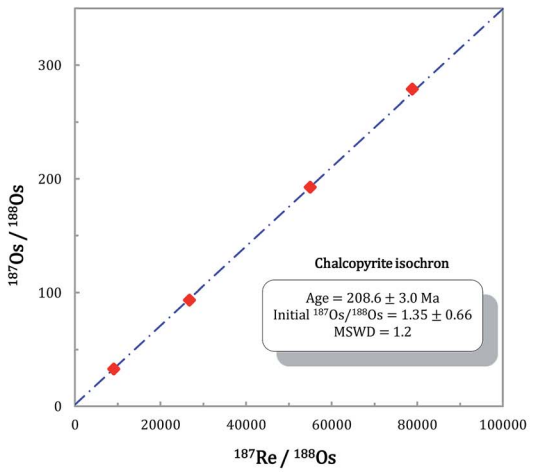

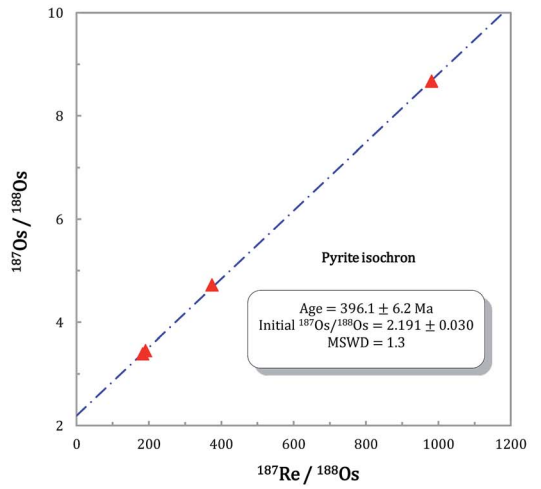

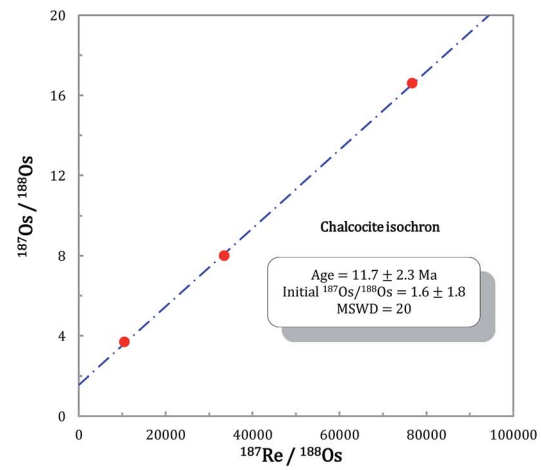

Fig. 5 $^{187}Re/^{188}Os$ *versus* $^{187}Os/^{188}Os$ isochron diagram showing the ages of the sulfide samples analyzed during this study.

4. Conclusions

This study presented a method for the simultaneous determination of Re–Os and S isotopic compositions of single sample solutions. This method uses HCl–HNO_3 digestion in sealed Carius tubes to convert S^{2-} to SO_4^{2-}, thereby avoiding the loss of S and volatile Os oxides during digestion. This two-stage tandem column procedure offers significant improvements in the separation efficiency of S from matrix elements compared with conventional single cation resin exchange or single anion resin exchange methods. Quantitative recoveries of S (99.8%) and Re (99.7%) are essential to avoid the potential isotope fractionation of standards and samples during chemical processing. Our proposed method for the simultaneous determination of Re–Os and S isotopic compositions of samples could reduce the number of samples needed and improve sample throughput, furthering the possible application of the Re–Os and S isotopic systems to the dating of ore deposits and the geochemical tracing of metals and sulfur in metallogenic systems.

Conflicts of interest

There are no conflicts to declare.

Acknowledgements

Three anonymous reviewers are appreciated for their constructive and critical comments on the manuscript. We also thank Dr Xia Xiaoping for providing the S data of YD136-206 and Dr Zhao Peipei for conducting the S isotope analyses. This research was funded by the Strategic Priority Research Program (B) of the Chinese Academy of Sciences (XDB18000000), the Instruments and Equipment Functional Development and Technology Innovation Project of Chinese Academy of Sciences (CAS) for Li Jie, and the National Natural Science Foundation of China (grant 41673008). This is contribution No. IS-2534 from GIGCAS.

References

1 R. Mathur, J. Ruiz and F. Tornos, *Miner. Deposita*, 1999, **34**, 790–793.
2 R. M. Morelli, C. C. Bell, R. A. Creaser and A. Simonetti, *Miner. Deposita*, 2010, **45**, 461–480.
3 D. Selby, K. D. Kelley, M. W. Hitzman and J. Zieg, *Econ. Geol.*, 2009, **104**, 437–444.
4 H. J. Stein, J. W. Morgan and A. Scherstén, *Econ. Geol.*, 2000, **95**, 1657–1671.
5 K. Suzuki, H. Shimizu and A. Masuda, *Geochim. Cosmochim. Acta*, 1996, **60**, 3151–3159.
6 S. G. Tessalina and O. Y. Plotinskaya, *Ore Geol. Rev.*, 2017, **85**, 174–180.
7 R. J. Walker, J. W. Morgan, E. Hanski and V. F. Smolkin, *Ont. Geol. Surv. Spec. Vol.*, 1994, **5**, 343–355.
8 I. B. Butler, M. E. Böttcher, D. Rickard and A. Oldroyd, *Earth Planet. Sci. Lett.*, 2004, **228**, 495–509.
9 L. F. Yang, K. X. Shi, C. M. Wang, B. Wu, B. Du and J. Y. Chen, *Acta Petrol. Sin.*, 2016, **32**, 2392–2406.
10 E. Henjes-Kunst, J. G. Raith and A. J. Boyce, *Ore Geol. Rev.*, 2017, **90**, 52–62.

11 C. LaFlamme, D. Sugiono, N. Thébaud, S. Caruso and M. Fiorentini, *Geochim. Cosmochim. Acta*, 2018, **222**, 436–446.
12 Z. Y. Chu, Y. Yan, Z. Chen, J. H. Guo, Y. H. Yang, C. F. Li and Y. B. Zhang, *Geostand. Geoanal. Res.*, 2015, **39**, 151–169.
13 L. Qi, M. F. Zhou, J. F. Gao and Z. Zhao, *J. Anal. At. Spectrom.*, 2010, **25**, 585–589.
14 S. B. Shirey and R. J. Walker, *Anal. Chem.*, 1995, **67**, 2136–2141.
15 C. E. Rees, *Geochim. Cosmochim. Acta*, 1978, **42**, 383–389.
16 N. V. Grassineau, D. P. Mattey and D. Lowry, *Anal. Chem.*, 2001, **73**, 220–225.
17 S. A. Studley, E. M. Ripley, E. R. Elswick, M. J. Dorais, J. Fong, D. Finkelstein and L. M. Pratt, *Chem. Geol.*, 2002, **192**, 141–148.
18 J. Labidi, P. Cartigny, J. Birck, N. Assayag and J. Bourrand, *Chem. Geol.*, 2012, **334**, 189–198.
19 B. A. Wing and J. Farquhar, *Geochim. Cosmochim. Acta*, 2015, **170**, 266–280.
20 A. L. Zerkle, D. S. Jones, J. Farquhar and J. L. Macalady, *Geochim. Cosmochim. Acta*, 2016, **173**, 373–386.
21 S. Ono, B. Wing, D. Rumble and J. Farquhar, *Chem. Geol.*, 2006, **225**, 30–39.
22 S. Ono, N. S. Keller, O. Rouxel and J. C. Alt, *Geochim. Cosmochim. Acta*, 2012, **87**, 323–340.
23 P. R. Craddock, O. J. Rouxel, L. A. Ball and W. Bach, *Chem. Geol.*, 2008, **253**, 102–113.
24 A. Das, C. H. Chung, C. F. You and M. L. Shen, *J. Anal. At. Spectrom.*, 2012, **27**, 2088–2093.
25 G. Paris, A. L. Sessions, A. V. Subhas and J. F. Adkins, *Chem. Geol.*, 2013, **345**, 50–61.
26 G. Paris, J. S. Fehrenbacher and A. L. Sessions, *Geochem., Geophys., Geosyst.*, 2014, **15**, 1452–1461.
27 R. Clough, P. Evans, T. Catterick and E. H. Evans, *Anal. Chem.*, 2006, **78**, 6126–6132.
28 J. L. Fu, Z. C. Hu, J. W. Li, L. Yang, W. Zhang, Y. S. Liu, Q. Li, K. Q. Zong and S. L. Hu, *J. Anal. At. Spectrom.*, 2017, **32**, 2341–2351.
29 T. L. Yu, B. S. Wang, C. C. Shen, P. L. Wang and Y. G. Chen, *Anal. Chim. Acta*, 2017, **988**, 34–40.
30 J. Labidi, P. Cartigny and M. Moreira, *Nature*, 2013, **501**, 208–211.
31 J. Labidi, P. Cartigny, C. Hamelin, M. Moreira and L. Dosso, *Geochim. Cosmochim. Acta*, 2014, **133**, 47–67.
32 S. Ono, W. C. Shanks, O. J. Rouxel and D. Rumble, *Geochim. Cosmochim. Acta*, 2007, **71**, 1170–1182.
33 J. Labidia, P. Cartignya and M. G. Jackson, *Earth Planet. Sci. Lett.*, 2015, **417**, 28–39.
34 Y. Ueno, S. Aoyama, Y. Endo, F. Matsu'ura and J. Foriel, *Chem. Geol.*, 2015, **419**, 29–35.
35 J. Labidi, J. Farquhar, C. M. O. 'D. Alexander, D. L. Eldridge and H. Oduro, *Geochim. Cosmochim. Acta*, 2017, **196**, 326–350.
36 J. Labidi and P. Cartigny, *Earth Planet. Sci. Lett.*, 2016, **451**, 196–207.
37 D. A. Yang, G. Landais, N. Assayag, D. Widory and P. Cartigny, *Rapid Commun. Mass Spectrom.*, 2016, **30**, 897–907.
38 J. Farquhar and B. A. Wing, *Earth Planet. Sci. Lett.*, 2003, **213**, 1–13.
39 J. Farquhar, S. T. Kim and A. Masterson, *Earth Planet. Sci. Lett.*, 2007, **264**, 1–8.
40 B. A. Wing and J. Farquhar, *Geochim. Cosmochim. Acta*, 2015, **170**, 266–280.
41 R. A. Creaser, D. A. Papanastassiou and G. J. Wasserburg, *Geochim. Cosmochim. Acta*, 1991, **55**, 397–401.
42 J. Völkening, T. Walczyk and K. Heumann, *Int. J. Mass Spectrom. Ion Processes*, 1991, **105**, 147–159.
43 J. Li, X. Y. Jiang, J. F. Xu and L. F. Zhong, *Geostand. Geoanal. Res.*, 2014, **38**, 37–50.
44 Z. C. Wang and H. Becker, *Geostand. Geoanal. Res.*, 2014, **38**, 189–209.
45 F. Albarède and B. Beard, *Rev. Mineral. Geochem.*, 2004, **55**, 113–152.
46 A. Amrani, A. L. Sessions and J. F. Adkins, *Anal. Chem.*, 2009, **81**, 9027–9034.
47 D. T. Johnston, B. C. Gill, A. Masterson, E. Beirne, K. L. Casciotti, A. N. Knapp and W. Berelson, *Nature*, 2014, **513**, 530–533.
48 H. J. Stein, R. J. Markey, J. W. Morgan, A. D. Du and Y. L. Sun, *Econ. Geol.*, 1997, **92**, 827–835.
49 D. H. Huang, Y. H. Wang, F. J. Nie and X. J. Jiang, *Acta Geol. Sin.*, 1984, **3**, 252–264.
50 T. Ding, S. Valkiers, H. Kipphardt, P. De Bièvre, P. D. P. Taylor, R. Gonfiantini and R. Krouse, *Geochim. Cosmochim. Acta*, 2001, **65**, 2433–2437.
51 Y. A. Alfayfi, Master's degree thesis, University of Calgary, 2014.
52 X. W. Huang, X. F. Zhao, L. Qi and M. F. Zhou, *Chem. Geol.*, 2013, **347**, 3–19.
53 J. Zhang, L. Li, X. P. Long, S. L. Sun and L. Yin, *Geostand. Geoanal. Res.*, 2017, **41**, 649–658.